

## THE STAR-FORMATION MASS SEQUENCE OUT TO $Z = 2.5$

KATHERINE E. WHITAKER<sup>1</sup>, PIETER G. VAN DOKKUM<sup>1</sup>, GABRIEL BRAMMER<sup>2</sup>, MARIJN FRANX<sup>3</sup>

*Submitted to the Astrophysical Journal Letters*

### ABSTRACT

We study the star formation rate (SFR) - stellar mass ( $M_*$ ) relation in a self-consistent manner from  $0 < z < 2.5$  with a sample of galaxies selected from the NEWFIRM Medium-Band Survey. We find a significant non-linear slope of the relation,  $\text{SFR} \propto M_*^{0.6}$ , and a constant observed scatter of 0.34 dex, independent of redshift and  $M_*$ . However, if we select only blue galaxies we find a linear relation  $\text{SFR} \propto M_*$ , similar to previous results at  $z = 0$  by Peng et al. (2010). This selection excludes red, dusty, star-forming galaxies with higher masses, which brings down the slope. By selecting on  $L_{\text{IR}}/L_{\text{UV}}$  (a proxy for dust obscuration) and the rest-frame  $U-V$  colors, we show that star-forming galaxies fall in three distinct regions of the  $\log(\text{SFR})$ - $\log(M_*)$  plane: 1) actively star-forming galaxies with “normal” dust obscuration and associated colors (54% for  $\log(M_*) > 10$  at  $1 < z < 1.5$ ), 2) red star-forming galaxies with low levels of dust obscuration and low specific SFRs (11%), and 3) dusty, blue star-forming galaxies with high specific SFRs (7%). The remaining 28% comprises quiescent galaxies. Galaxies on the “normal” star formation sequence show strong trends of increasing dust attenuation with stellar mass and a decreasing specific SFR, with an observed scatter of 0.25 dex (0.17 dex intrinsic scatter). The dusty, blue galaxies reside in the upper envelope of the star formation sequence with remarkably similar spectral shapes at all masses, suggesting that the same physical process is dominating the stellar light. The red, low-dust star-forming galaxies may be in the process of shutting off and migrating to the quiescent population.

*Subject headings:* galaxies: evolution — galaxies: formation — galaxies: high-redshift

### 1. INTRODUCTION

Galaxies show a strong correlation between their star formation rate (SFR) and stellar mass ( $M_*$ ) from  $z = 0$  to the earliest observed epoch,  $z = 7$  (e.g., Brinchmann et al. 2004; Noeske et al. 2007; Elbaz et al. 2007; Daddi et al. 2007; Pannella et al. 2009; Magdis et al. 2010; González et al. 2010). On average, galaxies on this “star formation sequence” were forming stars at much higher rates in the distant universe relative to today (e.g., Madau et al. 1996); for a given mass, the SFR has been decreasing at a steady rate by a factor of  $\sim 30$  from  $z \sim 2$  to  $z = 0$  (Daddi et al. 2007), although it appears to be roughly constant from  $z \sim 7$  to  $z \sim 2$  (González et al. 2010). The star formation sequence is observed to have a roughly constant scatter out to  $z \sim 1$  (e.g., Noeske et al. 2007).

Generally, star formation is thought to be regulated by the balance between the rate at which cold gas is accreted onto the galaxy and feedback (e.g., Dutton et al. 2010; Bouché et al. 2010), whereas the relation between gas surface density and SFR surface density does not appear to change, at least out to the highest redshifts accessible to molecular gas studies (Daddi et al. 2010; Tacconi et al. 2010). The star formation sequence may be a natural consequence of ‘cold mode accretion’ (e.g., Birnboim & Dekel 2003), as the SFR is approximately a steady function of time and yields a relatively tight

relationship between SFR and  $M_*$ . Feedback may affect the slope of the star formation sequence, whereas the evolution of the normalization is thought to result from evolution in gas densities with redshift. The scatter in the star formation sequence may reflect variations in the gas accretion history, and is predicted to be insensitive to stellar mass, redshift and feedback efficiencies (Dutton et al. 2010).

With a wealth of multi-wavelength data, including ultraviolet (UV) to near-infrared (NIR) photometric surveys,  $H\alpha$  spectroscopic surveys, and mid- to far-infrared photometry from *Spitzer*/MIPS at  $24\mu\text{m}$ , *Herschel*/PACS  $70$ – $160\mu\text{m}$ , and *Herschel*/SPIRE  $250$ – $500\mu\text{m}$ , much work has been done to calibrate different SFR indicators over broad redshift ranges (e.g., Muzzin et al. 2010; Hwang et al. 2010; Wuyts et al. 2011a,b; Reddy et al. 2012). Uncertainties in the star formation sequence may now be dominated by selection effects and observational biases. Selection effects can be important, as it is well known that a significant fraction of galaxies have very low SFRs, well below the star formation sequence. Furthermore, there exists a population of dusty star-forming galaxies with similar rest-frame optical colors to these quiescent galaxies (e.g., Brammer et al. 2009). The selection of star-forming galaxies and the treatment of quiescent galaxies can influence the measured relation and its scatter.

With the accurate photometric redshifts and photometry of the NEWFIRM Medium-Band Survey (NMBS; Whitaker et al. 2011), we can now extend studies of the star formation sequence out to  $z = 2.5$  for the largest mass-complete sample of galaxies to date. In this letter, we study the evolution of the  $\log(\text{SFR})$ - $\log(M_*)$  relation from  $0 < z < 2.5$ , selecting star-forming galaxies in a

katherine.whitaker@yale.edu

<sup>1</sup> Department of Astronomy, Yale University, New Haven, CT 06511

<sup>2</sup> European Southern Observatory, Alonso de Córdova 3107, Casilla 19001, Vitacura, Santiago, Chile

<sup>3</sup> Sterrewacht Leiden, Leiden University, NL-2300 RA Leiden, The Netherlands

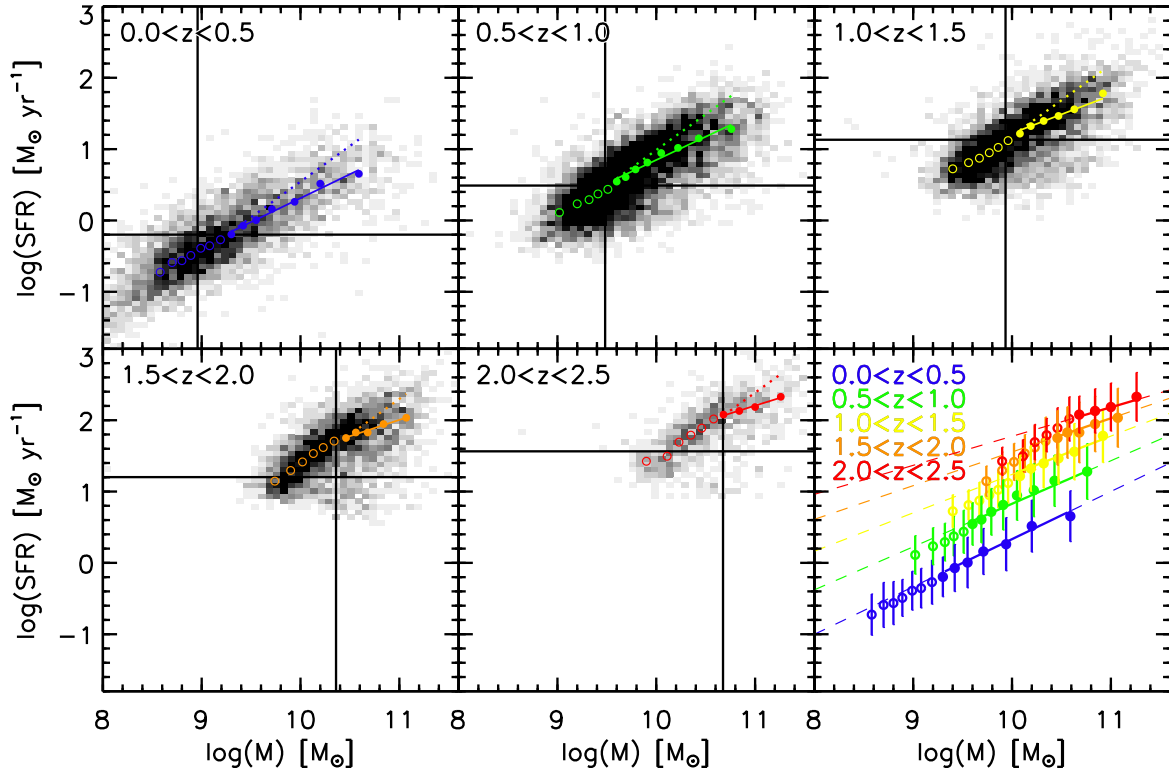


FIG. 1.— The SFR-mass sequence for star-forming galaxies has a non-linear slope out to  $z = 2.5$  (dotted line is linear). The running medians and scatter are color-coded by redshift, with a power law fit above the mass and SFR completeness limits (solid lines in bottom, right panel).

way that is independent from the SFR indicator. We show that star-forming galaxies with different colors and  $L_{\text{IR}}/L_{\text{UV}}$  ratios occupy different regions of the  $\log(\text{SFR})\text{-}\log(M_*)$  plane.

We assume a  $\Lambda$ CDM cosmology with  $\Omega_M=0.3$ ,  $\Omega_\Lambda=0.7$ , and  $H_0=70 \text{ km s}^{-1} \text{ Mpc}^{-1}$  throughout the paper.

## 2. DATA AND SAMPLE SELECTION

Our sample of galaxies is drawn from the NMBS (Whitaker et al. 2011). This survey employs a new technique of using five medium-bandwidth NIR filters to sample the Balmer/4000Å break from  $1.5 < z < 3.5$  at a higher resolution than the standard broadband NIR filters. The combination of the medium-band NIR images with deep optical medium and broadband photometry and IRAC imaging over  $0.4 \text{ deg}^2$  results in accurate photometric redshifts ( $\Delta z/(1+z) \lesssim 2\%$ ), rest-frame colors and stellar population parameters. The SFRs presented in this paper are based in part on *Spitzer*-MIPS fluxes at  $24\mu\text{m}$  that are derived from the S-COSMOS (Sanders et al. 2007) and FIDEL<sup>4</sup> surveys. A comprehensive overview of the survey can be found in Whitaker et al. (2011). The stellar masses used in this work are derived using FAST (Kriek et al. 2009), with Bruzual & Charlot (2003) models that assume a Chabrier (2003) initial mass function (IMF), solar metallicity, exponentially declining star formation histories

and dust extinction following the Calzetti et al. (2000) extinction law.

The SFRs are determined by adding the UV and IR emission,  $\text{SFR}_{\text{UV+IR}} = 0.98 \times 10^{-10} (L_{\text{IR}} + 3.3L_{2800})$  (Kennicutt 1998), adapted for the Kroupa IMF by Franx et al. (2008), accounting for the unobscured and obscured star formation, respectively. We adopt a luminosity-independent conversion from the observed  $24\mu\text{m}$  flux to the total IR luminosity ( $L_{\text{IR}} \equiv L(8\text{--}1000\mu\text{m})$ ), based on a single template that is the log average of Dale & Helou (2002) templates with  $1 < \alpha < 2.5$ , following Wuyts et al. (2008); Franx et al. (2008); Muzzin et al. (2010), and in good median agreement with recent *Herschel*/PACS measurements by Wuyts et al. (2011a). The luminosities at  $2800\text{\AA}$  ( $L_{2800}$ ) are derived directly from the best-fit template to the observed photometry, using the same methodology as the rest-frame colors (see Brammer et al. 2011).

With accurate rest-frame colors, it is possible to isolate “clean” samples of star-forming and quiescent galaxies using two rest-frame colors out to high redshifts (Labbé et al. 2005; Wuyts et al. 2007; Williams et al. 2009; Ilbert et al. 2009; Brammer et al. 2011; Whitaker et al. 2011). The quiescent galaxies have strong Balmer/4000Å breaks, characterized by red  $U\text{-}V$  colors and bluer  $V\text{-}J$  colors relative to dusty star-forming galaxies at the same  $U\text{-}V$  color.

Whitaker et al. (2011) demonstrated that there is a clear delineation between star-forming and quiescent galaxies with the NMBS data set. Quiescent galaxies are

<sup>4</sup> <http://irsa.ipac.caltech.edu/data/SPITZER/FIDEL/>

identified using the criteria  $U - V > 0.8 \times (V - J) + 0.7$ ,  $U - V > 1.3$  and  $V - J < 1.5$ , and they are excluded from the bulk of this analysis. The sample of star-forming galaxies is selected independent of the SFR indicator and stellar population synthesis model parameters, enabling an unbiased measurement of the star formation sequence.

### 3. THE STAR FORMATION SEQUENCE

Figure 1 shows the star formation sequence,  $\log(M_\star)$ – $\log(\text{SFR})$ , in five redshift bins out to  $z = 2.5$ . The greyscale represents the density of points for star-forming galaxies selected in Section 2, with the running median and biweight scatter color-coded by redshift. The mass completeness limits are estimated from the 90% point-source completeness limits derived from the unmasked simulations by Whitaker et al. (2011). The SFR completeness limits correspond to the  $3\sigma$   $24\mu\text{m}$  detection limit ( $17.6 \mu\text{Jy}$ ) at the highest redshift of each bin. All  $24\mu\text{m}$  detections  $< 1\sigma$  are replaced with the  $1\sigma$  upper limit, resulting in a flattened tail of the  $\log(\text{SFR})$ – $\log(M_\star)$  relation at low  $M_\star$ , where the samples are incomplete.

#### 3.1. Quantifying the Star Formation Sequence

The running medians and dispersions are measured for all star-forming galaxies, and those above the mass and SFR completeness limits are indicated with filled symbols in Figure 1 and fit with a power law,

$$\log(\text{SFR}) = \alpha(z)(\log M_\star - 10.5) + \beta(z) \quad (1)$$

We find that the slope  $\alpha$  gradually evolves with redshift, while the normalization  $\beta$  has a stronger evolution:

$$\alpha(z) = 0.70 - 0.13z \quad (2)$$

$$\beta(z) = 0.38 + 1.14z - 0.19z^2 \quad (3)$$

Previous studies have found hints of a similar trend for the slope to flatten toward  $z \sim 1$  or high  $M_\star$  (e.g., Noeske et al. 2007; Karim et al. 2011; Wuyts et al. 2012). Although the slope is consistent with a gradual evolution toward shallower values, we note that the highest redshift bins are only for galaxies with stellar masses  $> 10^{10.7} M_\odot$ , due to incompleteness at lower masses. We will address this issue in Section 3.2.

The average SFR of star-forming galaxies steeply declines from  $z = 2.5$  to the present day, changing by roughly  $0.2 \text{ dex Gyr}^{-1}$ , confirming the results of previous studies (e.g. Noeske et al. 2007; Elbaz et al. 2007, etc.). The normalization  $\beta$  decreases by a factor of 4 from  $z = 2$  to  $z = 0$ , while the global SFR density has decreased a factor of 6 over the same interval (Hopkins & Beacom 2006). We note that  $\beta(z)$  is the evolution in the specific SFR ( $\text{sSFR} \equiv \text{SFR}/M_\star$ ) at  $\log(M_\star) = 10.5$  (consistent with Elbaz et al. 2007; Daddi et al. 2008; Pannella et al. 2009; Damen et al. 2009; Magdis et al. 2010, etc.).

Interestingly, the scatter in the star formation sequence is observed to be roughly constant at  $\sim 0.34 \text{ dex}$ , both with redshift and stellar mass, consistent with the idea that it reflects variations in the gas accretion history. The observed scatter agrees with results from Noeske et al. (2007) at  $z < 1$ , although we note that there are hints of a lower scatter for the most massive galaxies in our highest redshift bin. We find that these results are robust against changes in sample selection. If we include all galaxies

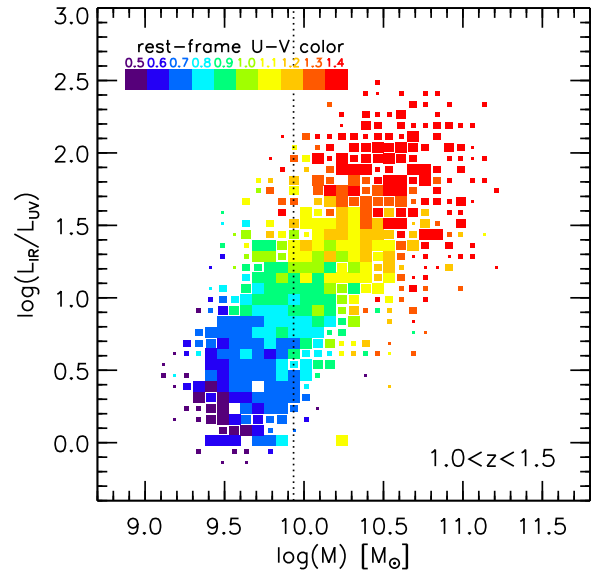


FIG. 2.— More massive star-forming galaxies have higher  $\log(L_{\text{IR}}/L_{\text{UV}})$  ratios and redder rest-frame  $U-V$  colors, suggesting increasing amounts of dust attenuation. The dotted line is the mass-completeness limit.

(quiescent and star-forming) with  $> 1\sigma$  detections, the scatter increases by 0.07–0.11 dex.

#### 3.2. The Effects of Dust Attenuation

Previous studies have noted that dust attenuation is a strong function of stellar mass (e.g., Reddy et al. 2006, 2010; Pannella et al. 2009; Wuyts et al. 2011b), where the most massive galaxies are more highly obscured. We find a similar trend with the NMBS data in Figure 2; higher mass galaxies have larger  $L_{\text{IR}}/L_{\text{UV}}$  ratios. The SFRs derived from  $L_{2800}$  alone exhibit a flat trend with stellar mass (or even hints of less UV flux toward higher  $M_\star$ ), whereas SFRs derived from  $L_{\text{IR}}$  show a strong trend with  $M_\star$ . The star formation-mass relation only materializes when dust attenuation is properly taken into account.

From Figure 2, we also see that the average rest-frame  $U-V$  color of star-forming galaxies becomes redder with increasing stellar mass (and increasing  $L_{\text{IR}}/L_{\text{UV}}$ ). The red colors may be attributed to dust, although older stellar populations have similarly red colors. It is notoriously difficult to differentiate between subtle age and dust effects with a single color alone. However, because  $L_{\text{IR}}$  is independent of the rest-frame color measurements, we can isolate galaxies with red colors predominantly due to dust.

The strong dependence of  $L_{\text{IR}}/L_{\text{UV}}$  and the rest-frame  $U-V$  color on stellar mass raises the question of whether the star formation sequence can be “resolved” into distinct populations of star-forming galaxies. We first consider the following two samples at  $1.0 < z < 1.5$  (where we have a large number of galaxies at the high-mass end while maintaining a modest mass-completeness level): 1) blue star-forming galaxies with little dust obscuration ( $U - V < 1.3$ ,  $\log(L_{\text{IR}}/L_{\text{UV}}) < 1.5$ ), and 2) dusty red star-forming galaxies ( $U - V > 1.3$ ,  $\log(L_{\text{IR}}/L_{\text{UV}}) > 1.5$ ).

When we select blue star-forming galaxies, similar to Peng et al. (2010), the slope of the star formation se-

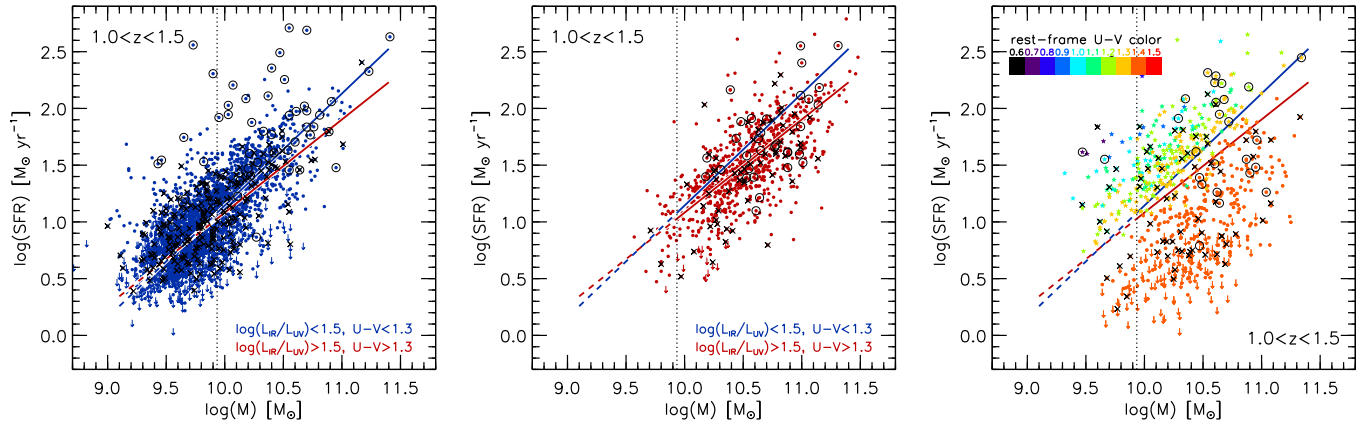


FIG. 3.— The  $\log(\text{SFR})$ - $\log(M_*)$  relation for blue star-forming galaxies with low dust has a best-fit slope close to unity (left), whereas dusty, red star-forming galaxies follow a shallower slope (middle). Although selected independent of their measured SFRs and  $M_*$ , blue, dusty galaxies and red, low-dust galaxies lie above and below the star formation sequence, respectively (right). X-ray detections are indicated with a black open circles, and those galaxies without X-ray coverage are indicated with crosses.

quence is close to unity and the observed scatter decreases to 0.25 dex (left panel of Figure 3). However, dusty red star-forming galaxies are an increasing fraction of the massive galaxy population toward  $z = 2$  (e.g., Whitaker et al. 2010). The middle panel of Figure 3 shows the star formation sequence for galaxies with red colors that we attribute to dust due to the high  $L_{\text{IR}}/L_{\text{UV}}$  ratios. This population of galaxies has a similarly small observed scatter of 0.25 dex, but a shallower slope of  $\sim 0.8$ .

While it has been shown that higher mass galaxies tend to have lower sSFRs (e.g., Zheng et al. 2007), previous studies have not always distinguished between actively star-forming and passive stellar populations. Here, we find that *among* actively star-forming galaxies, the star formation sequence for red dusty (high-mass) galaxies has a shallower slope, as compared to that for blue low-dust (low-mass) galaxies. This result implies that both massive quiescent and star-forming galaxies have lower sSFRs and hence older ages.

### 3.3. What causes galaxies to be outliers on the star formation sequence?

We next consider the sample of star-forming galaxies with “anomalous” combinations of rest-frame color and  $L_{\text{IR}}/L_{\text{UV}}$  ratios to determine where these galaxies lie in the SFR- $M_*$  plane. We stress that we are not *selecting* these galaxies to be outliers in the  $\log(\text{SFR})$ - $\log(M_*)$  plane, rather to be unusual in their observed color and dust properties. The galaxies with red rest-frame colors and low  $L_{\text{IR}}/L_{\text{UV}}$  ratios fall in the lower envelope of the star formation sequence (right panel of Figure 3). These low sSFR galaxies may be in the process of shutting down star formation. Similarly, we identify galaxies that have blue colors but high  $L_{\text{IR}}/L_{\text{UV}}$  ratios. We find that dusty, blue galaxies have high sSFRs, predominantly residing in the upper envelope of the star formation sequence. This suggests that they are in a starburst phase and/or may have active galactic nuclei (AGN).

To search for signatures of AGN, we match the NMBS catalogs within a 1 arcsecond radius to the X-ray point source catalogs from the AEGIS-X survey (Laird et al. 2009) and the Chandra COSMOS survey (Elvis et al. 2009). Those galaxies with counterparts in the X-ray

catalogs are indicated with open circles in Figure 3. We find that the fraction of galaxies with X-ray detections is  $\sim 4\%$  in all populations of star-forming galaxies, implying that the central black holes may become active at any stage of star formation (e.g., Santini et al. 2012). Interestingly, X-ray detected galaxies tend to be outliers in the  $\log(\text{SFR})$ - $\log(M_*)$  plane (see Figure 3), probably because a fraction of the  $24\mu\text{m}$  emission is not associated with star formation, as assumed.

## 4. DISCUSSION

We find that the star formation sequence is not linear, with  $\text{SFR} \propto M_*^{0.6}$  and a constant observed scatter of 0.34 dex. If we only select blue galaxies, however, we do find a linear relation, similar to Peng et al. (2010). This selection removes red, dusty star-forming galaxies at the high mass end, which have a shallower slope. We note that Pannella et al. (2009) also find a slope close to unity at  $z \sim 2$ , however this may be a result of the “BzK” selection. Here, we are able to analyze the star formation sequence with a mass-complete sample of galaxies.

By accounting for the ratio of  $L_{\text{IR}}/L_{\text{UV}}$  (a proxy for dust) and the rest-frame  $U-V$  colors of star-forming galaxies, we develop a simple picture that describes how galaxies populate the  $\log(\text{SFR})$ - $\log(M_*)$  plane. We have identified four distinct populations: 1) quiescent galaxies (28% for  $\log(M_*) > 10$  at  $1.0 < z < 1.5$ ), 2) actively star-forming galaxies with “normal” colors and associated  $L_{\text{IR}}/L_{\text{UV}}$  ratios (54%), 3) red star-forming galaxies with low  $L_{\text{IR}}/L_{\text{UV}}$  ratios and low sSFRs (11%), and 4) blue star-forming galaxies with high  $L_{\text{IR}}/L_{\text{UV}}$  ratios and sSFRs (7%).

Among the galaxies that populate the “normal” star formation sequence, we see a continuous sequence of increasing levels of dust attenuation with increasing stellar mass and a decreasing slope in the  $\log(\text{SFR})$ - $\log(M_*)$  relation, implying decreasing sSFRs with stellar mass (Figure 4). Wuyts et al. (2011b) observed similar trends across the SFR- $M_*$  plane, where  $L_{\text{IR}}/L_{\text{UV}}$  increases along the sequence and at a given  $M_*$  towards high SFRs. The dependence of sSFR on  $M_*$  appears to introduce a slight curvature to the star formation sequence. A power-law fit to *all* star-forming populations results in an observed scatter that is 0.09 dex larger than that of the “normal”

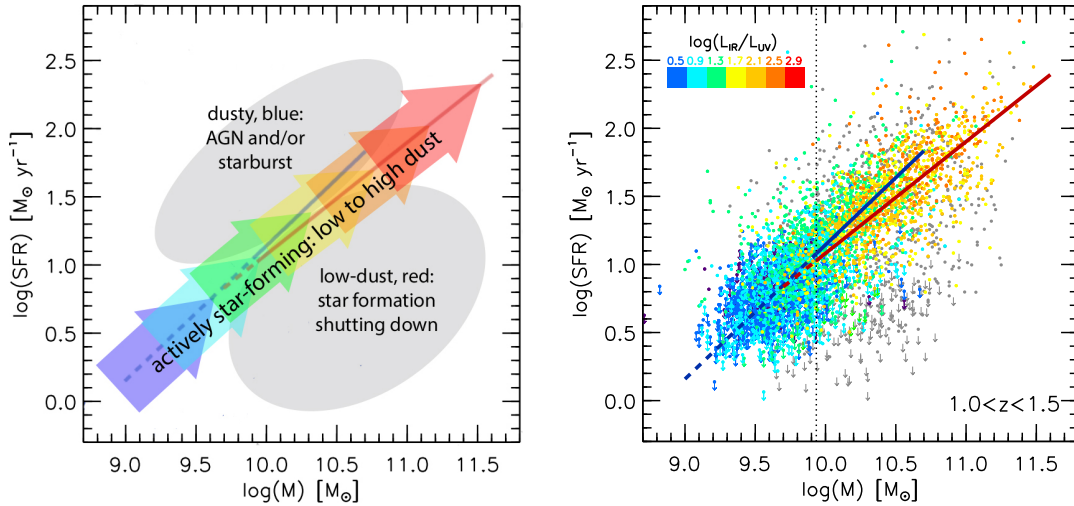


FIG. 4.— A cartoon (left) and observed (right) view of how star-forming galaxies populate the  $\log(\text{SFR})$ - $\log(M_*)$  plane, with 54% of all galaxies residing on the “normal” star formation sequence, showing increasing amounts of dust (higher  $L_{\text{IR}}/L_{\text{UV}}$  ratios) and lower sSFRs (shallower slope) towards higher stellar mass. 7% of galaxies have blue colors and high  $L_{\text{IR}}/L_{\text{UV}}$  ratios, falling in the upper envelope (grey). 11% of galaxies have low  $L_{\text{IR}}/L_{\text{UV}}$  ratios and red colors, populating the lower envelope (also grey).

sequence, with a significantly shallower slope of  $\sim 0.6$ . We note that some models predict slopes that are too steep compared to the observations (e.g., Bouché et al. 2010; Dutton et al. 2010); it is possible that discrepancies between the inferred SFRs may be alleviated if the stellar IMF is systematically weighted toward more high-mass star formation in rapidly star-forming galaxies (Narayanan & Davé 2012).

The observed scatter of the “normal” star formation sequence is 0.25 dex, which includes contributions from both random and systematic errors. We estimate the average random scatter by perturbing the  $24\mu\text{m}$  photometry and photometric redshifts within the  $1\sigma$  error bars for 100 realizations, finding a small contribution of  $\sim 0.05$  dex. Additionally, about 0.08 dex scatter is introduced because the average SFR evolves within the redshift bin. Finally, uncertainties in the conversion from  $24\mu\text{m}$  flux to  $L_{\text{IR}}$  introduce  $\sim 0.15$  dex scatter (Marcillac et al. 2006), although we note that this value is quite uncertain (e.g., Wuyts et al. 2011a). In total, we estimate that random and systematic errors introduce 0.18 dex scatter to the star formation sequence, from which we estimate the intrinsic scatter to be 0.17 dex. Semi-analytic models predict an even smaller scatter ( $0.12 \pm 0.1$  dex). However, the model scatter may be underestimated due to a simplified treatment of the halo mass accretion history. Cosmological hydrodynamical simulations by Dekel et al. (2009) find a scatter of up to 0.3 dex in the gas accretion rates on to galaxies in  $10^{12} M_{\odot}$  haloes at  $z = 2.5$ . If this scatter translates linearly into scatter in the SFRs, this may reconcile the differences between the models and observed scatter.

To bolster the cartoon view presented in Figure 4, we additionally consider the composite SEDs of normal star-forming galaxies in bins of stellar mass. Due to the increasing levels of dust attenuation, we see a clear evolution of the composite SEDs in Figure 5. On average, the most massive star-forming galaxies have characteristically dusty spectral shapes, with a  $2175\text{\AA}$  dust feature evident, whereas lower stellar mass galaxies have decreasing amounts of dust obscuration. We note that we see

similar trends at higher and lower redshifts, but are unable to make robust statements due to incompleteness.

We speculate that the small fraction of dusty, blue galaxies are mainly starbursts, as very few appear to be associated with X-ray sources. Remarkably, we see that the spectral shapes of these galaxies are all very similar, irrespective of stellar mass (upper right panel in Figure 5). This suggests that the same physical process is dominating the stellar light, possibly a merger driven starburst.

While 28% of galaxies with  $\log(M_*) > 10$  have already quenched their star formation at  $1 < z < 1.5$ , we find that 11% may be in the process of shutting down star formation. These galaxies have red colors and low  $L_{\text{IR}}/L_{\text{UV}}$  ratios, occupying the lower envelope of the star formation sequence. We compare the composite SEDs of these red, low-dust star-forming galaxies to that of quiescent galaxies at the same stellar mass and redshift (solid lines in bottom right panel of Figure 5). These galaxies have similar rest-frame  $V-J$  colors to quiescent galaxies, but somewhat bluer rest-frame  $U-V$  colors, consistent with the idea that they are in the process of shutting down star formation and may soon migrate to the red sequence.

By studying four distinct populations of galaxies selected from the NMBS, we have demonstrated that quantifying the observed properties of the star formation sequence and how the sequence evolves with time requires a thorough understanding of the selection techniques and biases. A consequence of the strong dependence of dust attenuation on stellar mass is that measurements of the star formation sequence will depend critically on the sample selection. The gradual evolution we measure of the slope of the star formation sequence toward shallower values at high- $z$  is driven by the combination of the curvature of the “normal” star formation sequence and the evolution of the mass-completeness limits with redshift. An in-depth analysis of the physical properties of these galaxies and comparisons between the observations and models will help constrain the physical mechanism driving this potential curvature and the outliers from the star formation sequence.

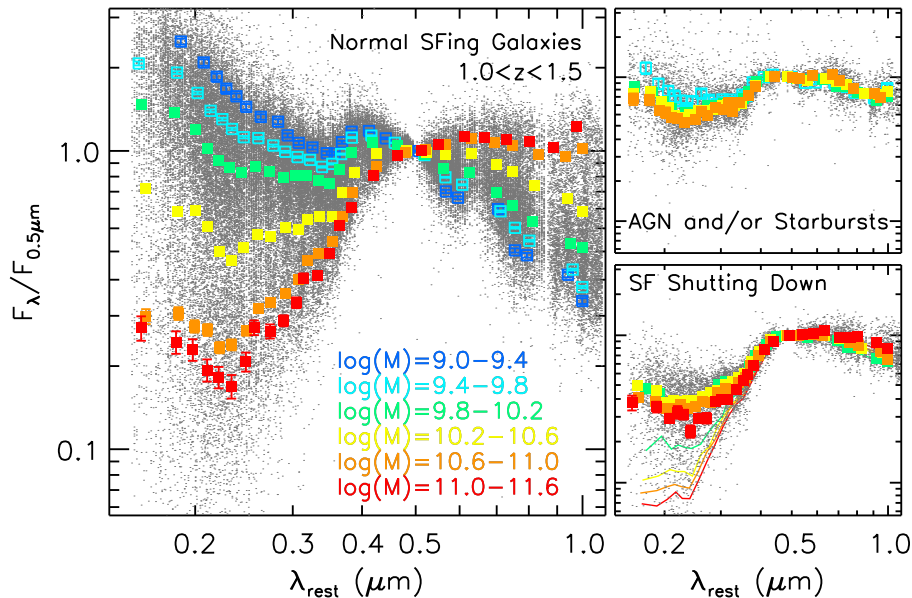


FIG. 5.— The rest-frame composite SEDs of galaxies on the “normal” star formation sequence (left) showing increasing levels of dust attenuation with stellar mass. The spectral shape of dusty, blue galaxies appears to be independent of stellar mass (upper right). Galaxies in the process of shutting off their star formation (bottom right) show larger amounts of rest-frame UV emission relative to quiescent galaxies at the same stellar mass and redshift (solid lines).

We thank the NMBS collaboration for their contribution to this work, and the COSMOS and AEGIS teams for the release of high quality multi-wavelength data

sets to the community. Support from NSF grant AST-0807974 and NASA grant NNX11AB08G is gratefully acknowledged.

*facilities:* Mayall (NEWFIRM)

#### REFERENCES

- Birnboim, Y., & Dekel, A. 2003, MNRAS, 345, 349  
 Bouché, N., Dekel, A., Genzel, R., et al. 2010, ApJ, 718, 1001  
 Brammer, G. B., Whitaker, K. E., van Dokkum, P. G., et al. 2011, ApJ, 739, 24  
 —. 2009, ApJ, 706, L173  
 Brinchmann, J., Charlot, S., White, S. D. M., et al. 2004, MNRAS, 351, 1151  
 Bruzual, G., & Charlot, S. 2003, MNRAS, 344, 1000  
 Calzetti, D., Armus, L., Bohlin, R. C., et al. 2000, ApJ, 533, 682  
 Chabrier, G. 2003, PASP, 115, 763  
 Daddi, E., Bournaud, F., Walter, F., et al. 2010, ApJ, 713, 686  
 Daddi, E., Dannerbauer, H., Elbaz, D., et al. 2008, ApJ, 673, L21  
 Daddi, E., Dickinson, M., Morrison, G., et al. 2007, ApJ, 670, 156  
 Dale, D. A., & Helou, G. 2002, ApJ, 576, 159  
 Damen, M., Labbé, I., Franx, M., et al. 2009, ApJ, 690, 937  
 Dekel, A., Birnboim, Y., Engel, G., et al. 2009, Nature, 457, 451  
 Dutton, A. A., van den Bosch, F. C., & Dekel, A. 2010, MNRAS, 405, 1690  
 Elbaz, D., Daddi, E., Le Borgne, D., et al. 2007, A&A, 468, 33  
 Elvis, M., Civano, F., Vignali, C., et al. 2009, ApJS, 184, 158  
 Franx, M., van Dokkum, P. G., Schreiber, N. M. F., et al. 2008, ApJ, 688, 770  
 González, V., Labbé, I., Bouwens, R. J., et al. 2010, ApJ, 713, 115  
 Hopkins, A. M., & Beacom, J. F. 2006, ApJ, 651, 142  
 Hwang, H. S., Elbaz, D., Magdis, G., et al. 2010, MNRAS, 409, 75  
 Ilbert, O., Capak, P., Salvato, M., et al. 2009, ApJ, 690, 1236  
 Karim, A., Schinnerer, E., Martínez-Sansigre, A., et al. 2011, ApJ, 730, 61  
 Kennicutt, Jr., R. C. 1998, ARA&A, 36, 189  
 Kriek, M., van Dokkum, P. G., Labbé, I., et al. 2009, ApJ, 700, 221  
 Labbé, I., Huang, J., Franx, M., et al. 2005, ApJ, 624, L81  
 Laird, E. S., Nandra, K., Georgakakis, A., et al. 2009, ApJS, 180, 102  
 Madau, P., Ferguson, H. C., Dickinson, M. E., et al. 1996, MNRAS, 283, 1388  
 Magdis, G. E., Rigopoulou, D., Huang, J.-S., et al. 2010, MNRAS, 401, 1521  
 Marcellac, D., Elbaz, D., Chary, R. R., et al. 2006, A&A, 451, 57  
 Muzzin, A., van Dokkum, P., Kriek, M., et al. 2010, ApJ, 725, 742  
 Narayanan, D., & Davé, R. 2012, ArXiv e-prints  
 Noeske, K. G., Weiner, B. J., Faber, S. M., et al. 2007, ApJ, 660, L43  
 Pannella, M., Carilli, C. L., Daddi, E., et al. 2009, ApJ, 698, L116  
 Peng, Y.-j., Lilly, S. J., Kovač, K., et al. 2010, ApJ, 721, 193  
 Reddy, N., Dickinson, M., Elbaz, D., et al. 2012, ApJ, 744, 154  
 Reddy, N. A., Erb, D. K., Pettini, M., et al. 2010, ApJ, 712, 1070  
 Reddy, N. A., Steidel, C. C., Fadda, D., et al. 2006, ApJ, 644, 792  
 Sanders, D. B., Salvato, M., Aussel, H., et al. 2007, ApJS, 172, 86  
 Santini, P., Rosario, D. J., Shao, L., et al. 2012, A&A, 540, A109  
 Tacconi, L. J., Genzel, R., Neri, R., et al. 2010, Nature, 463, 781  
 Whitaker, K. E., Labbé, I., van Dokkum, P. G., et al. 2011, ApJ, 735, 86  
 Whitaker, K. E., van Dokkum, P. G., Brammer, G., et al. 2010, ApJ, 719, 1715  
 Williams, R. J., Quadri, R. F., Franx, M., et al. 2009, ApJ, 691, 1879  
 Wuyts, S., Förster Schreiber, N. M., Genzel, R., et al. 2012, ArXiv e-prints  
 Wuyts, S., Förster Schreiber, N. M., Lutz, D., et al. 2011a, ApJ, 738, 106  
 Wuyts, S., Förster Schreiber, N. M., van der Wel, A., et al. 2011b, ApJ, 742, 96  
 Wuyts, S., Labbé, I., Franx, M., et al. 2007, ApJ, 655, 51  
 Wuyts, S., Labbé, I., Schreiber, N. M. F., et al. 2008, ApJ, 682, 985  
 Zheng, X. Z., Bell, E. F., Papovich, C., et al. 2007, ApJ, 661, L41